Acta Technica *62* (2017), No. 7A, 109–124 

# Target image detection based on improved BOF algorithm and similarity measurement

Lishao Huang[1]

**Abstract.** A detection technique of digital image forgery based on local descriptor of multi-resolution Weber was proposed on the basis of Weber's Law pertinent to deficiencies such as low accuracy, weak adaptability and simplicity of current detection algorithm of digital image forgery. WLD feature was extracted from chrominance channel of images, and more characteristic quantities could be extracted compared with single resolution through introduction of multi-resolution; meanwhile, WLD histogram could be formed under different resolutions in directions of differential excitation and gradient through optimization of WLD parameters; then classification could be conducted with SVM. Experimental data indicates: WLD of multi-resolution has better detection result compared with single resolution, and WLD of multi-resolution has better detection performance in detection of splicing forgery images and copying-moving forgery images. Forgery detection experiment in many image data bases indicates: WLD of multi-resolution has better detection result compared with single resolution, and WLD of multi-resolution has better detection performance in detection of splicing forgery images and copying-moving forgery images.

**Key words.** Similarity measure of images, Target detection; Image forgery, Support vector machine (SVM), Feature matching.

## 1. Introduction

With rapid development of multi-media equipment and image editing technology, people can easily conduct forgery handling such as editing and modification on images, and it can be achieved that forgery images cannot be observed, which leads to popular questioning on authenticity and completeness of images. Especially images impose great influence on people when they are used in mass media such as newspaper, magazine and Internet, etc or in the field of medical diagnosis or as court evidence, producing serious damage to the whole society[1, 2]. So adulteration

[1]School of Electronics and Information Engineering, Hunan University of Science and Engineering, Yong Zhou, 425199, China

detection of digital images is an very important research subject.

Detection technology of image forgery can be divided into two categories including active technology and passive technology, and active technology includes embed watermark technology and digital signature technology, etc[3,4]. Passive detection is mainly blind detection technology, and images are certified through analyzing image content and detailed information. For active detection method has limits such as needing to embed signature beforehand and lowering image effect, etc, blind detection technology has better practicability and research value.

The most common blind forgery methods are copying-moving forgery (CMF) and splicing forgery (SF). Certain part of an image is copied and moved to another area of the same image for CMF to hide or add new content and create forgery images. A part of the same image or different images is cut, and then it is combined into the same image[5] through pre-treatment such as edge smoothing for image splicing. A forgery detection method of copying-pasting based on non-negative matrix factorization was proposed by AOH[6], etc, and simulation result indicated that the algorithm had higher detection precision. But the shortcoming of the method is that image after geometric transformation cannot be detected. A blind forensic method of slicing positioning based on the original image of matrix estimation of color filter was designed by Wang Bo[7], etc, and experimental result verifies the excellence of the algorithm. But the calculation amount is large and time-space complexity is high. A forgery detection method of undecimated wavelet transform (UWT) was proposed by G. Muhammad[8], etc, and approximate value and detailed coefficient of overlapped blocks of images were calculated to seek for similarity among blocks. But UWT does not adapt to JPEG compression and rotation and zoom of images, so it is of little adaptability.

## 2. Detection algorithm in this thesis

Fig. 1 is flow chart of forgery detection system of copying-moving images, Firstly, input colored image is transformed into YCrCb model, and the color is protected in forms of brightness and chromaticity. In Phase II, image feature can be extracted according to chrominance components (Cr or Cb) and the fact that sensitivity of human eye to chromaticity is weaker than brightness. In the methods of this thesis, local descriptor of Weber is WLD histogram obtained from calculation under resolutions C1, C2, C3 according to Weber's Law[9] applied in image texture features. WLD histogram of multi-resolution is formed in combination with WLD histogram of single resolution calculated to indicate image features, and WLD of multi-resolution has better recognition effect compared with that of single resolution.

Finally, images are divided into true image and forgery image by SVM according to classification standard.

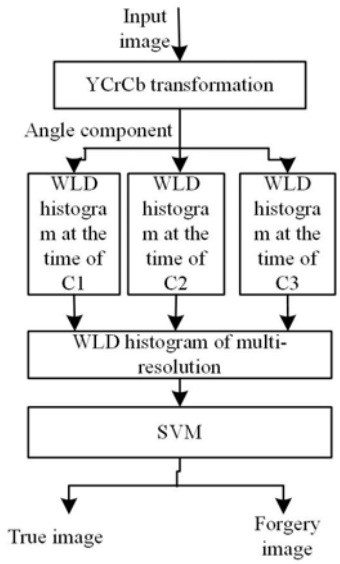


Fig. 1. Flow chart of forgery detection of images in this thesis

### *2.1. RGB Transformation of chrominance component of RGB image*

Image forgery is commonly conducted on RGB color image. So chrominance space can be a powerful way of detecting forgery images for forgery detection on digital images. Chrominance space is introduced into image detection, and it is composed of hue Cr and saturability Cb[10-11]. Cr reflects difference between red part of input signal and signal brightness value, while Cb reflects difference between blue part of input signal and signal brightness value. Function of transformation RGB image to YCrCb color model is as follows:

$$Y = 0.299R + 0.587G + 0.114B + 0.5\,, \tag{1}$$

$$Cr = 0.713(R - Y) + 128.5\,, \tag{2}$$

$$Cb = 0.564(B - Y) + 128.5\,. \tag{3}$$

Color is stored in forms of brightness and chromaticity for YCrCb color space. For sensitivity of human eye to chromaticity is weaker than brightness, so tapering trace will be left on chrominance channel even though image tampering looks very natural. Thus feature extraction method of chrominance component is more effective on forgery detection.

### *2.2. Feature extraction*

Image feature is important information to analyze forgery image and true image. So feature extraction is an important step of image recognition system. For forgery detection of WLD image of multi-resolution proposed in this thesis, WLD is based on sensitivity of human eye on original stimulus intensity change and essential description to extract image feature. For WLD is aimed at image feature extraction, it has great advantage[12] on edge detection. WLD is composed of differential excitation (D) and direction ($\phi$). The difference threshold of the feeling changes with change of initial stimulus amount:

$$\frac{\nabla x}{x} = C\,. \tag{4}$$

Where increased threshold amount is $\nabla x$, and $x$ is original stimulus amount, and $C$ is constant.

While difference excitation (D) indicates intensity change of each pixel point of the image, and difference excitation of pixel point $P_c$ is indicated as $D(P_c)$, and the calculation is as follows:

1. Difference value of pixel point $P_c$ and its surrounding pixel points are calculated through $(f_{00})$ filter, as shown in Fig. 2:

$$K_s^{00} = \sum_{i=0}^{N-1} (\nabla p_i) = \sum_{i=0}^{N-1} (p_i - p_c) \tag{5}$$

Where $P_i$ is ith neighboring pixel point of $P_c$, and N is number of neighboring pixel points.

2. Then calculate ratio of difference value of current pixel intensity input from filters $(f_{00})$ and $(f_{01})$:

$$I = \frac{K_s^{00}}{K_s^{01}} = \sum_{i=0}^{N-1} \frac{p_i - P_c}{P_c}\,. \tag{6}$$

So differential excitation $D(P_c)$ of pixel point $P_c$ is as follows:

$$D(P_c) = \arctan\left[\sum_{i=0}^{N-1} \frac{p_i - P_c}{P_c}\right]\,. \tag{7}$$

Set up the direction of pixel point $P_c$ to $\phi(P_c)$, then $WLD$ direction is gradient direction:

$$\phi(P_c) = \arctan(\frac{K_s^{11}}{K_s^{10}})\,. \tag{8}$$

Where $K_s^{11}$ and $K_s^{10}$ are respectively output value of filters $f_{11}$ and $f_{10}$.

$$K_s^{10} = p_5 - p_1, K_s^{11} = p_7 - p_3\ . \tag{9}$$

$T$ main directions can be quantized by directional gradient, and definition of measured function is as follows:

$$\Phi_t = f_q(\phi') = \frac{2t\pi}{T}\,. \tag{10}$$

$$t = \mathrm{mod}\left(\left|\frac{\phi'}{2\pi/T} + \frac{1}{2}\right|, T\right)\,. \tag{11}$$

Where $\phi'$ is corresponding mapping value of $\phi$, and mapping function $f$: $\phi \to \phi'$:

$$\phi' = \arctan 2(K_s^{11}, K_s^{10}) + \pi \tag{12}$$

$$\arctan 2(K_s^{10}, K_s^{11}) = \begin{cases} \varphi & K_s^{11} > 0 \; and \; K_s^{10} > 0\,, \\ \varphi + \pi & K_s^{11} > 0 \; and \; K_s^{10} > 0\,, \\ \varphi - \pi & K_s^{11} < 0 \; and \; K_s^{10} < 0\,, \\ \varphi & K_s^{11} < 0 \; and \; K_s^{10} > 0\,. \end{cases} \tag{13}$$

Where $\phi \in [-\pi/2, \pi/2]$ and $\phi' \in [0, 2\pi]$. If $T = 8$, then $T$ main directions $\Phi_t = t\pi/4$, $(t = 0, 1, 2..., T-1)$, so quantized interval of $\Phi_t$ is $[\Phi_t - \pi/T, \Phi_t + \pi/T]$.

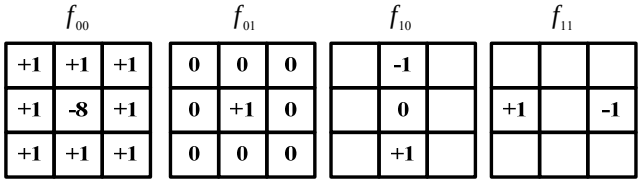


Fig. 2. Filter window in WLD

So differential excitation is calculated through WLD, thus grey value change between current pixel and its neighboring pixel in the image can be judged; and directional information of image texture change can be intuitively reflected according to directional information of grey value change of current pixel of WLD gradient direction.

### *2.3. WLD histogram*

Two-dimension WLD histogram $\{WLD(D(P_c), \Phi_t)\}$ can be achieved after calculating differential excitation $D(P_c)$ and gradient direction $\Phi_t$ according to models (7) and (11). $P_c = 0, 1, ., N-1$, $t = 0, 1, ., T-1$, where N is dimension number of images, and T is number of main directions. So in two-dimension histogram, y-coordinate is main direction D, and x-coordinate is $\Phi$, as shown in Fig. 3. There are three parameters imposing influence on detection result in WLD histogram: predominant directional vector $(T)$, segment number of differential excitation $(M)$, segment number $(S)$ of sub-histogram.

In WLD of multi-resolution proposed in this thesis, differential excitation and gradient direction are calculated in three different areas of $(8, 1)$, $(16, 2)$ and $(24, 3)$.

The first figure in the bracket indicates number of neighboring pixel, and the second figure indicates radius value[9] of current pixel. Gradient direction of differential excitation of local descriptor of Weber is calculated with filter windows of different scales to obtain local descriptor of Weber in different scales. $WLD$ of multi-resolution is formed with local descriptors of Weber calculated in different scales.

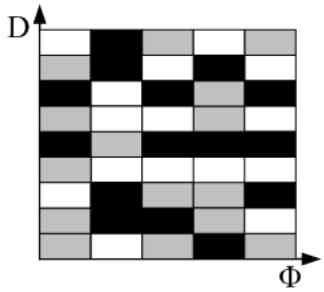


Fig. 3. WLD histogram

### *2.4. Classifier*

Classified learning on extracted forgery image features is conducted and authenticity of images is judged[13] with classified function with classified function of SVM to increase forgery detection precision. As a kind of machine learning technology, $SVM$ includes two phases of training and testing. Feature value can be input into $SVM$ for classification. $SVM$ Classifier can obtain good performance[14] through radius basis function. If its training set is $(a_i, b_i)$, $i = 1, 2, ..., M$, $a_i \in R$, $b_i \in \{-1, +1\}$, $a_i$ is feature vector of training set, and $b_i$ is classification of training set, then its aim is to establish a new classifier with the lowest false drop rate from current models. A optimal hyper-plane $g_a$ is established according to $SVM$: $g_a = C^T x + C_0$, then expression of classification plane is as flows:

$$C^T x + C_0 = 0\,. \tag{14}$$

If all sets are needed to satisfy condition: $|g_a| \geq 1$, then linear judgment function shall be normalized. Where, it shall be satisfied if it is close to classification plane: $|g_a| = 1$, and classification interval is $2/\left\|C^T\right\|$. Minimum $\left\|C^T\right\|$ needs to be figured out to maximize classification interval, so optimal classification plane shall satisfy the following condition to classify all sets accurately:

$$b_i\left[C^T x + C_0\right] - 1 \geq 0 \quad i = 1, 2, ..., M\,. \tag{15}$$

It can be evolved into solving minimum of model (16) to obtain optimal classification plane:

$$f(C^T) = \frac{1}{2}\left\|C_T\right\|^2\,. \tag{16}$$

Lagrange function is defined as follows to obtain optimal value of model (16):

$$L(C^T, C_0, \alpha) = \frac{1}{2}\left\|C^T\right\| - \sum_{i=1}^{M} \alpha_i \left\{b_i \left[C^T x_i + C_0\right] - 1\right\}. \tag{17}$$

Where, Lagrange constant $\alpha_i > 0$

Lagrange minimum of $C^{\mathrm{T}}$ and $C_0$ are solved respectively through partial differential technology. Namely the problem of solving minimum is transformed into solving maximum of model (18) function.

$$\varphi(\alpha) = \sum_{i=1}^{M} \alpha_i - \frac{1}{2} \sum_{i,j=1}^{M} \alpha_i \alpha_j b_i b_j (a_i a_j). \tag{18}$$

Optimal solution $\alpha_i^*$ is obtained through calculation, and corresponding optimal weight vector $C_T^*$ and optimal bias vector $C_o^*$ can be solved through the following equations:

$$C_T^* = \sum_{j=1}^{M} \alpha_j^* b_j a_j. \tag{19}$$

$$C_o^* = b_i - \sum_{j=1}^{M} b_i \alpha_j^* (b_j \bullet a_j). \tag{20}$$

Where, $j \in \left\{j \left| \alpha_j^* > 0 \right.\right\}$, and optimal hyper-plane $C_T^* x + C_0^* = 0$.

Corresponding optimal classification function $f(x)$:

$$\begin{aligned} f(x) &= sgn(C_T^* x + C_0^*) \\ &= sgn\left\{\sum_{j=1}^{M} b_i \alpha_j^* (x_j \bullet x) + C_0^*\right\} \quad x \in R^n \end{aligned} \tag{21}$$

Fig. 4 is WLD histogram of true image and splicing as well as forgery image in Cr channel with multi-resolution. Fig. 5 is multi-resolution WLD histogram obtained from Cr chrominance component of true image and copying-moving forgery image with unchanged tapering area. Similarly, Fig. 6 is multi-resolution WLD histogram obtained from Cr chrominance component of true image and copying-moving forgery image with rotated tapering area. It can be seen that forgery forms such as splicing, copying-moving and rotation, etc can be effectively detected for the algorithm in this thesis, so it has strong robustness.

## 3. Experiment and discussion

Forgery detection performance of copying and moving in this thesis is tested in CASIA database, and dimension of all images is 384×256 in JPEG format in this

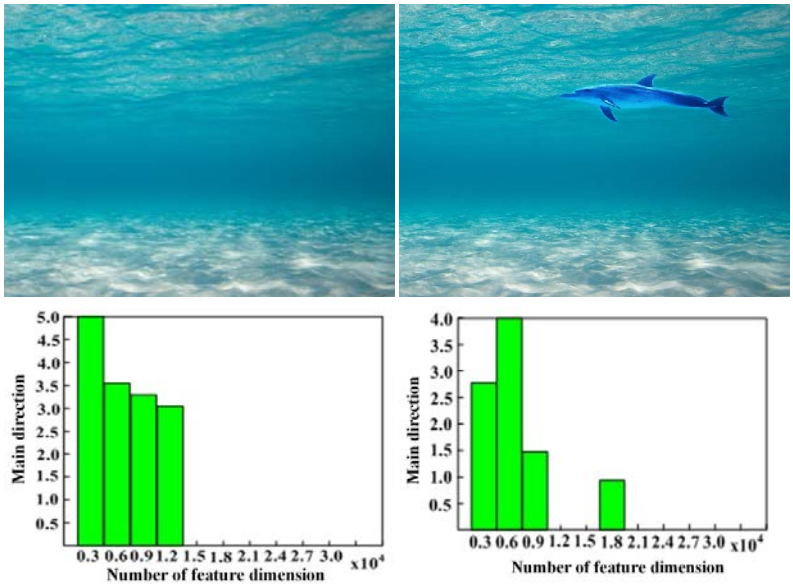


(a) True image (b) Forgery image

Fig. 4. WLD histogram of original image and splicing image

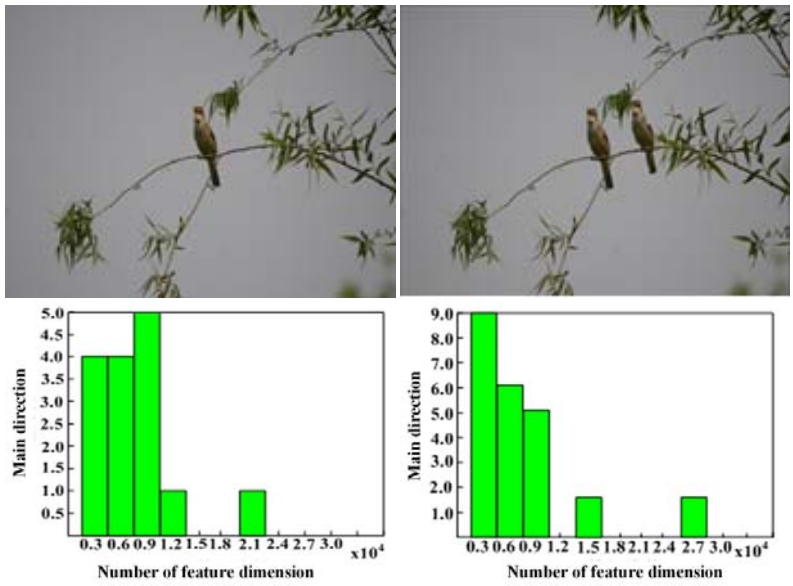


(a) True image (b) Forgery image

Fig. 5. WLD histogram of original image and copied & forgery image

database. Original images are divided into eight classifications: animal, scenery, person, plant, nature, architecture, texture and article, and images are selected in

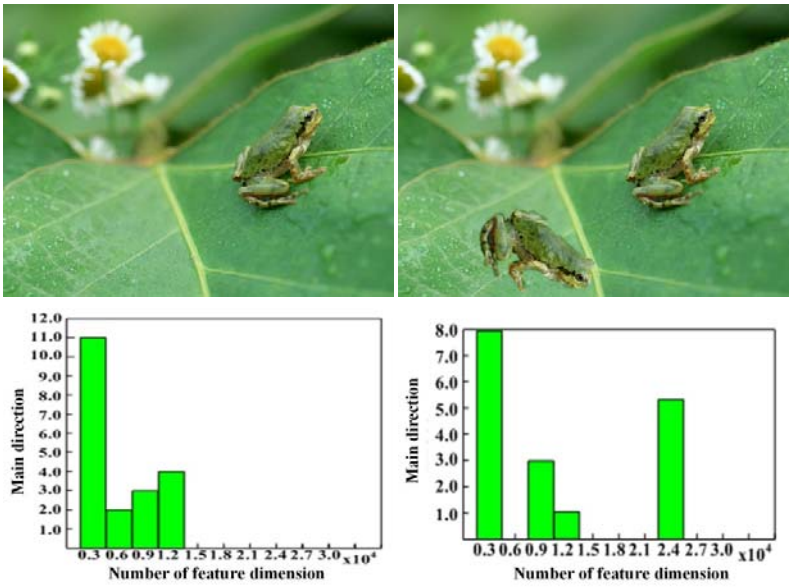


(a) True image (b) Forgery image

Fig. 6. WLD histogram of original image and rotation forgery image

each group at random as training object. Tapering includes handling of copying and pasting; it also includes geometric rotation, such as rotation, zooming, etc. Forgery image can be produced with PS software. Common forgery types are splicing and copying-moving. There are 390 true images and 459 tapered images in splicing image set, and there are 261 true images and 462 forgery images in copying-moving set.

Detection performance of the algorithm is assesses with specificity, sensitivity and area under the curve. Sensitivity $S_n$ indicates accuracy of correct classification, and its calculation indication is as follows:

$$S_n = \frac{TP}{TP + FN} * 100\% \,. \tag{22}$$

Specificity $S_p$ is accuracy of false classification, and its indication is as follows:

$$S_p = \frac{TN}{FP + TN} * 100\% \,. \tag{23}$$

Precision $A_c$ is ratio of correct classification images to total images, it is indicated as follows:

$$A_c = \frac{TP + TN}{TP + FN + FP + TN} * 100\% \,. \tag{24}$$

Where, $TP$ is number of tampered images classified into tampered images correctly, and $FN$ is number of tampered images classified into true images falsely. $FP$ is number of true images classified into tampered images fa of lsely, and $TN$ is number of true images classified into true images correctly.

AUC is a standard to measure the quality of a classification model. Commonly its value is between 0.5 and 1, and larger value indicates better classification performance.

Firstly, RGB image is transformed into YCrCb chrominance space, and then WLD feature is extracted from chrominance component. In the same scale of $C_1(8,1)$, $C_2(16,2)$ and $C_2(16,2)$, $SVM$ classification performance of RBF kernel function is assessed in ten-folding bracketing method on combination $C_4$ of $C_1$ and $C_2$, combination $C_5$ of $C_1$ and $C_3$, combination $C_6$ of $C_2$ and $C_3$, combination $C_7$ of $C_1$, $C_2$ and $C_3$.

### *3.1. Parameter optimization of* $WLD$

Fig. 7 indicates influence of parameters $T$, $M$ and $S$ of multi-resolution $WLD$ in $Cr$ channel on detection precision. A parameter is changed for each time, and it can be seen from Fig. 8 that the best result is achieved when T=4, M=4 and S=20.

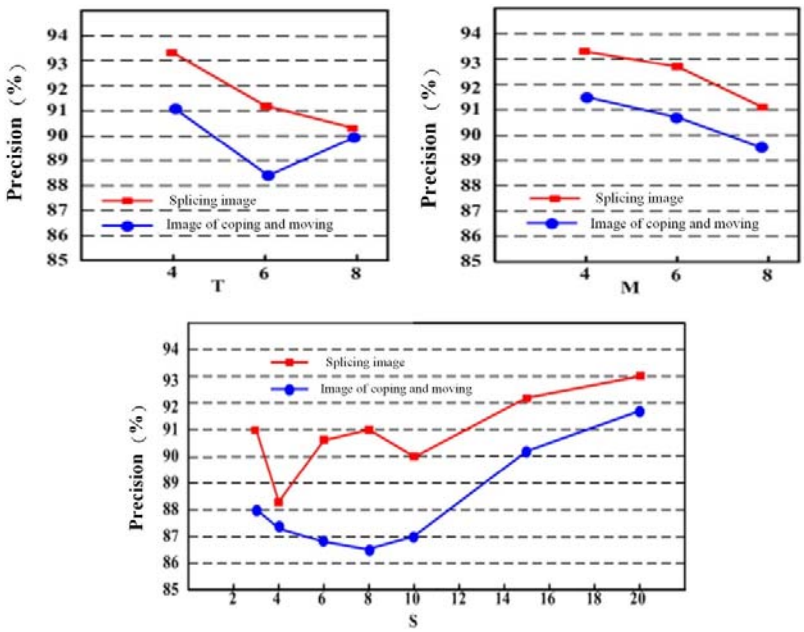


Fig. 7. Influence of parameters T, M and S on algorithm precision of this thesis

### *3.2. Splicing detection*

Splicing detection result of $WLD$ in different resolutions in chrominance channels of Cr and Cb is indicated in Fig. 8. It can be found in Fig. 8 that detection performance in channel of Cb is lower than that of Cr when resolution is the same, and detection precision in channel $C_2$ is the best in single resolution $(C_1, C_2, C_3)$; detection precision of C7 in combination of $C_1, C_2, C_3$ is the best in multi-resolution.

Precision of $C_7$ in channel Cr can reach 91.82%, and its precision in channel Cb can reach 88.92%. It is mainly due to 320 feature quantities produced by $WLD$ at the time of single resolution, and $320 \times 3 = 960$ feature quantities produced by $C_7$. So It can be seen image detection performance of multi-resolution WLD is better than that of single resolution from experiments.

Afterwards, detection precision of multi-resolution $C_7$ is respectively observed in channels of chrominance and brightness. Detection result of splicing image of chrominance component, brightness component and combination of chrominance and brightness is shown in Table 1, and it can be seen from the table that detection precision of combination of Cr and Cb is the best (up to 92.38% and AUC is 0.92. This is due to the fact that sensitivity of human eye to chrominance is weaker than brightness. Even though it looks very natural for image tampering, there is still tampering trace in channel of chrominance, so it is more effective to adopt feature extraction method of chrominance component for forgery detection. Disturbance of a single component can be reduced in combination with channels of Cr and Cb, thus detection result can be more accurate.

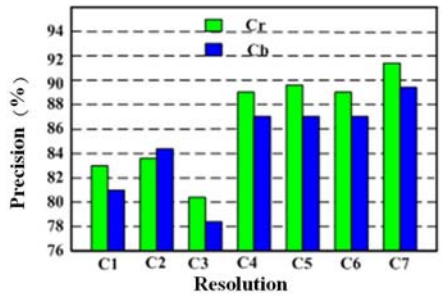


Fig. 8. Detection precision of WLD in different resolutions in channel of chrominance

Table 1. SF detection result of WLD in all channels of C7

| Channel | AC/% | AUC | Sn/% | Sp/% | Feature quantity |
|---|---|---|---|---|---|
| Y | 54.34 | 0.51 | 92.45 | 7.17 | 960 |
| Cb | 88.92 | 0.88 | 91.21 | 89.04 | 960 |
| Cr | 91.82 | 0.90 | 92.31 | 91.13 | 960 |
| Cr+Cb | 93.28 | 0.92 | 92.87 | 93.75 | 1920 |

### *3.3. Forgery detection of copying and moving*

CMF detection result of WLD in different resolutions in chrominance channels of Cr and Cb is indicated in Fig. 9. In most cases, performance of Cr is better than Cb. In most resolutions, performance of C7 is the best, and the precision in channel of Cr can reach 90.87%, while it can reach 86.92% in Cb channel. It can be found that CMF detection precision is lower than splicing detection precision in comparison of Fig. 8 and Fig. 9. The main reason is that the copied area is from

the same image in CMF forgery image, and features such as noise and frequency, etc are almost the same as the original image, while splicing images are from different images of different background modes. So detection of splicing image is easier than CMF, and detection precision is higher.

Detection result of CMF image of chrominance component, brightness component and component combination of chrominance and brightness is shown in Table 2, and it can be found from the table that detection precision of combination of Cr and Cb is the best (can reach 91.88%), and AUC is 0.89.

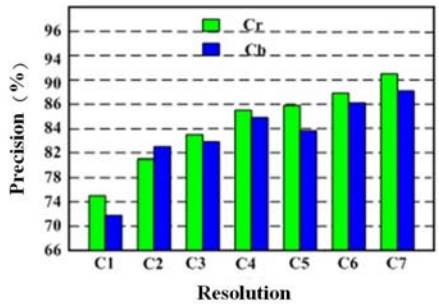


Fig. 9. Detection precision of WLD in different resolutions in chrominance channel

Table 2. CMF detection result of all channels of C7

| Channel | AC/% | AUC | Sn/% | Sp/% | Feature quantity |
|---|---|---|---|---|---|
| Y | 69.11 | 0.60 | 93.18 | 35.46 | 960 |
| Cb | 86.92 | 0.85 | 93.79 | 77.28 | 960 |
| Cr | 90.48 | 0.88 | 95.91 | 81.12 | 960 |
| Cr+Cb | 91.88 | 0.89 | 96.92 | 83.293 | 1920 |

### *3.4. Forgery detection of changed tampering area type*

Result of multi-resolution (C7) of splicing image detection based on changed tampering areas is indicated in Table 3. Here are four change types: (1) transformation of tampering area; (2) zooming of tampering area; (3) rotation of tampering area; (4) invariableness of tampering area. It can be found from Table 3 that detection precision of rotation forgery of tampering area is the lowest in these four types, while detection precision of zooming type is the highest. Image detection of copying-moving based on changed tampering area is shown in Table 4, and detection effect of unchanged tampering area is the best.

Table 3. SF detection result based on changed tampering area

| Type | True/forgery | Channel | Accuracy% | AUC |
|---|---|---|---|---|
| Transformation | 43/45 | Cb | 81.37 | 0.81 |
| | | Cr | 87.62 | 0.83 |
| | | Cb+Cr | 86.36 | 0.82 |
| Zooming | 155/179 | Cb | 84.82 | 0.86 |
| | | Cr | 90.12 | 0.91 |
| | | Cb+Cr | 90.61 | 0.91 |
| Rotation | 22/22 | Cb | 74.40 | 0.77 |
| | | Cr | 62.80 | 0.58 |
| | | Cb+Cr | 77.26 | 0.79 |
| Invariableness | 162/170 | Cb | 84.15 | 0.84 |
| | | Cr | 89.14 | 0.90 |
| | | Cb+Cr | 89.27 | 0.90 |

Table 4. CMF detection result based on changed copying area

| Type | True/forgery | Channel | Accuracy/% | AUC |
|---|---|---|---|---|
| Transformation | 14/14 | Cb | 61.10 | 0.57 |
| | | Cr | 74.20 | 0.63 |
| | | Cb+Cr | 54.96 | 0.54 |
| Adjustment | 27/27 | Cb | 42.38 | 0.47 |
| | | Cr | 66.78 | 0.65 |
| | | Cb+Cr | 63.16 | 0.67 |
| Rotation | 9/9 | Cb | 32.10 | - |
| | | Cr | 32.40 | - |
| | | Cb+Cr | 20.56 | - |
| Invariableness | 200/404 | Cb | 86.98 | 0.84 |
| | | Cr | 90.20 | 0.87 |
| | | Cb+Cr | 90.67 | 0.89 |

### *3.5. Image forgery detection based on changed tampering shape*

Detection result of multi-resolution of image splicing and CMF detection based on shape of different tampering areas is shown in Table 5and Table 6. There are four types of changed tampering areas: roundness, rectangle, triangle (only pertinent to CMF) and any shape. Precision of any shape can reach 92.72% at the time of detection of splicing image, and precisions of roundness and rectangle are respectively 95.34% and 75.88%. In most cases in CMF detection, precision of Cr channel is higher that that of channel of combined chrominance.

Table 5. SF forgery detection result of different tampering shapes

| Type | True/forgery | Channel | Accuracy/% | AUC |
|---|---|---|---|---|
| Any | 370/427 | Cb | 89.55 | 0.92 |
| | | Cr | 92.47 | 0.91 |
| | | Cb+Cr | 92.72 | 0.93 |
| Roundness | 14/14 | Cb | 85.67 | 0.85 |
| | | Cr | 80.73 | 0.82 |
| | | Cb+Cr | 95.34 | 0.91 |
| Rectangle | 19/19 | Cb | 55.85 | 0.64 |
| | | Cr | 75.64 | 0.85 |
| | | Cb+Cr | 75.88 | 0.75 |

Table 6. Detection result of CMF image of different tampering shapes

| Type | True/forgery | Channel | Accuracy/% | AUC |
|---|---|---|---|---|
| Any shape | 105/101 | Cb | 80.12 | 0.80 |
| | | Cr | 87.36 | 0.86 |
| | | Cb+Cr | 83.41 | 0.82 |
| Roundness | 108/108 | Cb | 77.62 | 0.79 |
| | | Cr | 79.34 | 0.78 |
| | | Cb+Cr | 79.86 | 0.84 |
| Rectangle | 136/136 | Cb | 76.32 | 0.75 |
| | | Cr | 82.89 | 0.81 |
| | | Cb+Cr | 81.02 | 0.80 |
| Triangle | 97/97 | Cb | 77.53 | 0.75 |
| | | Cr | 82.62 | 0.82 |
| | | Cb+Cr | 80.29 | 0.79 |

### *3.6. Comparison with Literature [17]*

Comparison on chrominance channel is conducted on the algorithm in this thesis and algorithm in Literature [17]. Comparison result is shown in Table 7, and precision of the methods proposed in this thesis is higher than that in Literature [17] on splicing and CMF detection. Literature [17] is mainly based on local binary mode, and the size of each pixel and neighboring pixel is only compared the algorithm in this thesis excluding change amplitude of grey value; directional information of image texture change can be reflected intuitively via calculating gradient direction of image through WLD, while directional information of image is not involved for local binary mode; besides, influence of single chrominance component can be reduced and detection precision of image forgery is raised through multi-resolution.

Table 7. Algorithm comparison with Literature [17]

| Forgery type | Algorithm in this thesis | Algorithm of Literature [17] |
|---|---|---|
| Splicing | 93.28% | 79.90% |
| Copying-moving | 91.88% | 76.30% |

Forgery image is detected through multi-resolution WLD in the algorithm of this thesis. Test of different resolutions is conducted in channel of chrominance component, and the result indicates detection result in Cr channel is better; detection precision of this algorithm on splicing images is higher than that of images of copying-moving; multi-resolution has better detection effect compared with single resolution. In type change and shape change of copying area, test of changed tampering type and changed shape is respectively conducted on splicing images and images of copying-moving, thus influence of different type and shape of tampering area on image forgery detection is obtained. Compared with the algorithm proposed in Literature [17], detection precision of splicing in this thesis and CMF forgery are both higher that that of Literature [17], indicating good detection performance of multi-resolution WLD proposed in this thesis.

## 4. Conclusion

Detection technique of image forgery of local descriptor for Weber of coupling multi-resolution for SVM is proposed to increase accuracy precision of image forgery detection and strengthen adaptability of algorithm pertinent to problems of low accuracy of image forgery detection and weak adaptability, etc. Image is firstly is transformed to YCrCb model and kept in forms of brightness and chrominance, and then image feature is extracted according to chrominance component and the fact that sensitivity of human eye to chrominance is weaker than brightness; than WLD calculation model can be established according to differential excitation and gradient direction of current pixel to judge grey value change and texture change of images; WLD parameter is analyzed and optimized to form WLD histogram with differential excitation and gradient direction of pixel in different resolutions; finally classification algorithm of SVM is introduced to conduct classified learning of extracted forgery images.

## Acknowledgement

Yongzhou science and Technology Bureau directive science and technology plan project (permanent branch, [2015]9, item number: 16);

Hunan University of Science and Engineering general science research project (16XKY052);

Supported by key subjects of computer application technology, Hunan University of Science and Engineering.

**References**


[1] C. H. Wu, Y. Zheng, W. H. Ip, et al.: *A flexible H.264/AVC compressed video watermarking scheme using particle swarm optimization based dither modulation*[J]. AEUE - International Journal of Electronics and Communications, *65* (2011), No. 1, 27–36.

[2] Y. Zheng, X. Zhang, G. Zhou, et al.: *Automatic PMD compensation experiment with particle swarm optimization and adaptive dithering algorithms for 10-gb/s NRZ and RZ formats*[J]. Quantum Electronics IEEE Journal of, *40* (2004), No. 4, 427–435.

[3] C. T. Hsieh, Y. K. Wu, W. J. Chung: *Digital watermarking system for halftone images based on particle swarm optimization*[C]// First IEEE International Conference on Ubi-Media Computing. IEEE, *2008* (2008), 201–206.

[4] C. H. Wu, Y. Zheng, W. H. Ip, et al.: *A flexible H.264/AVC compressed video watermarking scheme using particle swarm optimization based dither modulation*[J]. AEUE - International Journal of Electronics and Communications, *65* (2011), No. 1, 27–36.

[5] Y. Zheng, X. Zhang, Y. Shen, et al.: *Automatic polarization-mode dispersion compensation by a particle-swarm optimization method and adaptive dithering algorithm*[J]. Journal of the Optical Society of America B, *22*(2005), No. 2, 336–346.

[6] C. T. Hsieh, Y. K. Wu, W. J. Chung: *Digital watermarking system for halftone images based on particle swarm optimization*[C]// First IEEE International Conference on Ubi-Media Computing. IEEE, *2008* (2008), 201–206.

[7] G. Vahdati, M. Yaghoobi: *Fractal image compression based on spatial correlation and chaotic particle swarm optimization*[C]// International Conference on Computational Intelligence and Communication Networks. IEEE, *2011* (2011), 62–67.

[8] C. M. Li, Y. Wang, H. M. Gao, et al.: *Band Selection for Hyperspectral Image Classification Based on Improved Particle Swarm Optimization Algorithm*[J]. Advanced Materials Research, *889-890* (2014), No. 21, 1073–1077.

[9] D. U. Yazhi: *Digital image correlation method based on Newton-Raphson method and particle swarm optimization algorithm*[J]. Computer Engineering & Applications, *48* (2012), No. ,34, 184–189.

[10] Z. Liang, K. Wang, G. U. Guoqing, et al.: *Digital speckle image correlation method base on particle swarm optimization algorithm*[J]. Laser Technology. (2014).

[11] Y. Zhang, Z. M. Lu, D. N. Zhao: *An oblivious fragile watermarking scheme for images utilizing edge transitions in BTC bitmaps*[J]. Science China Information Sciences, *55* (2012), No. 11, 2570–2581.

[12] Bai H.: *Design of Non-Uniform Linear Array via Linear Programming and Particle Swarm Optimization and Studies on Phased Array Calibration*[J]. (2014)

[13] A. Mishra, A. Jain, A. J. Anurag Mishra: *Blind Watermarking Scheme for Un-Compressed Video Using RBF Neural Network*[J]. Ijrcct. (2013).

[14] H. S. Li, Q. Zhu, R. G. Zhou, et al.: *Multidimensional color image storage, retrieval, and compression based on quantum amplitudes and phases*[J]. Information Sciences, *273* (2014), No. 3, 212–232.

[15] C . Li , X. Song, Z. Liu, et al.: *A robust watermarking scheme based on maximum wavelet coefficient modification and optimal threshold technique*[J]. Journal of Electrical & Computer Engineering, *2015* (2015), 44.

[16] T. Currie, C. J. Lada, P. Plavchan, et al.: *The Last Gasp of Gas Giant Planet Formation: A Spitzer Study of the 5 Myr-old Cluster NGC 2362*[J]. Astrophysical Journal, *41* (2009), No. 297.


Received May 7, 2017